Environmental Science Nano

ROYAL SOCIETY OF CHEMISTRY

PAPER

View Article Online
View Journal | View Issue

Cite this: *Environ. Sci.: Nano*, 2022, **9**, 1106

Mechanistic analysis identifying reaction pathways for rapid reductive photodebromination of polybrominated diphenyl ethers using $BiVO_4$/BiOBr/Pd heterojunction nanocomposite photocatalyst†

Edward B. Miller,[a] Elsayed M. Zahran,[b] Marc R. Knecht [ac] and Leonidas G. Bachas [*ac]

Received 7th December 2021,
Accepted 13th January 2022

DOI: 10.1039/d1en01128f

rsc.li/es-nano

Polybrominated diphenyl ethers (PBDEs), previously incorporated in a wide variety of common products, can now be found throughout the environment. Because of their environmental persistence and the potential health hazards they pose to humans and wildlife, they have been added to the Stockholm Convention on Persistent Organic Pollutants, and they continue to be of significant concern. We report herein the first application of a nanocomposite catalyst consisting of a *m*-$BiVO_4$/BiOBr heterojunction surface-decorated with Pd nanoparticles in the photocatalytic reductive debromination of PBDEs using visible light. Specifically, this system demonstrated both rapid and complete debromination of 2,2′,4,4′-tetrabromodiphenyl ether (BDE-47), with an exceedingly large initial pseudo-first-order rate constant of 1.33 min^{-1}. Analysis of the reaction mechanism identified the stepwise degradation pathway to generate the final diphenyl ether product as well as the role of the alcohol-based sacrificial reagent. Such information provides routes towards new approaches for environmental remediation by identifying reaction pathways for common organic pollutants that remain challenging to degrade *via* sustainable methods.

Environmental significance

The ubiquitous environmental presence of polybrominated diphenyl ethers (PBDEs), endocrine-disrupting pollutants listed by the Stockholm Convention, continues to be a significant concern. We have found the nanocomposite material, *m*-$BiVO_4$/BiOBr/Pd, to be of superior efficacy in the sustainable photocatalytic degradation of PBDEs. This system relies on a nanoscale semiconductor heterojunction with Pd surface-decoration to accomplish photodebromination of the pollutant. One of the more recalcitrant congeners, BDE-47, was rapidly and completely debrominated to diphenyl ether. In addition, mechanistic details of the reaction were probed, which may further aid future advances.

Introduction

The environmental impact of persistent organic pollutants (POPs) continues to be an issue of significant concern.[1–3] Halogenated organic compounds (HOCs) constitute the majority of POPs targeted by the Stockholm Convention as having adverse environmental and health effects.[4] These include chlorinated pesticides such as dichlorodiphenyltrichloroethane (DDT), chlordane, aldrin, and dieldrin,[5] as well as polychlorinated biphenyls (PCBs), once used as dielectrics in capacitors and transformers, and as heat-transfer fluids.[6] Polybrominated diphenyl ethers (PBDEs, also known as BDEs) comprise an additional class of important HOCs that were added recently to the POPs identified in the Stockholm Convention.[7] These compounds were used extensively as flame-retardant additives in many consumer products until their use was banned; however,

[a] *Department of Chemistry, University of Miami, Coral Gables, Florida 33146, USA. E-mail: bachas@miami.edu*
[b] *Department of Chemistry, Ball State University, Muncie, Indiana 47306, USA*
[c] *Dr. J. T. Macdonald Foundation Biomedical Nanotechnology Institute, University of Miami, UM Life Science Technology Building, 1951 NW 7th Ave, Suite 475, Miami, Florida 33136, USA*

† Electronic supplementary information (ESI) available: Fig. S1. EDS spectra of (a) predominantly *m*-$BiVO_4$ region and (b) predominantly BiOBr region of the *m*-$BiVO_4$/BiOBr composite; Fig. S2. Adsorption of BDE-47 from 25 μM 1 : 1 EtOH/H_2O solution on $BiVO_4$/BiOBr/Pd particles stirring in darkness; Fig. S3. Propanal produced in the photodebromination of 100 μM BDE-3 with $BiVO_4$/BiOBr/Pd in 1 : 1 solution of 1-propanol/H_2O; Table S1. Reaction of BDE-3 with *m*-$BiVO_4$/BiOBr/Pd in different solvent systems; natural bond orbital (NBO) analysis of selected alcohols; Table S2. Select computed natural bond orbital (NBO) data for C1–C3 alcohols, from DFT calculations at the B3LYP/6-31G(d,p) level. See DOI: 10.1039/d1en01128f

because of their slow decomposition after disposal, there remains a legacy of persistent PBDEs throughout the environment.[8] Among the hazards associated with PBDEs is their ability to act as endocrine disruptors.[9–11] This is likely due to their structural similarity to the thyroid thyroxine hormones T_3 and T_4.[12] Moreover, evidence suggests that PBDEs can cause developmental neurotoxicity in animals.[13] Taken together, degradation of PBDEs is of great interest, where the development of new, sustainable approaches is desirable for long-term environmental remediation.

A variety of approaches have been developed for the remediation of various POPs, including biological degradation,[14–16] chemical oxidation,[17,18] reduction,[19,20] or a combination of both;[21] as well as photolysis,[22–25] radiolysis,[26] and thermal decomposition.[27] Recently, photocatalysis has emerged as a promising approach for the degradation of halogenated organic compounds.[28–30] In a semiconductor photocatalyst, solar irradiation leads to the formation of an exciton in the system, where the excited electrons and positively charged holes can be used for redox-based degradation of PBDEs.[31,32] To facilitate such a photocatalytic process, it is of critical importance that the charge carriers remain separated to avoid recombination, which is commonly found to be the rate limiting step in these reactions. One strategy for increasing carrier separation is the use of a p–n heterojunction architecture.[33] Depending upon the relative magnitude and position of the semiconductor bandgap, electrons and holes may accumulate on opposite sides of the junction, maximizing charge separation, leading to enhanced reactivity.

The photocatalytic degradation of halogenated compounds under aerobic conditions usually proceeds *via* oxidative mechanisms, in which holes, superoxide, and/or hydroxyl radicals play the major role in the decomposition of the organic contaminant.[34] For example, TiO_2 has been shown to photocatalytically degrade PBDEs in the presence of O_2 through a mechanism likely involving oxidation by hydroxyl radicals.[35] Such pathways, however, may give rise to oxidative intermediates, such as hydroxylated PBDEs (OH-PBDEs), polybrominated dibenzo-*p*-dioxins (PBBDs), and polybrominated dibenzofurans (PBDFs).[35] This can prove to be problematic as some of these oxidative byproducts are more toxic than the parent compound. PBBDs, in particular, are considered to be at least as toxic as the structurally analogous and hazardous polychlorinated benzodioxins (PCBDs).[36,37] While oxidative products can be more toxic, oxidation reactions could potentially fully degrade the POPs to CO_2 and H_2O, thereby limiting this oxidative byproduct concern; however, the photocatalyst would have to be sufficiently reactive over a long period to achieve such capabilities.

Reductive processes have also been proposed to decompose PCBs and PBDEs.[21,34,38–42] Such dehalogenation reactions do not generate dioxin byproducts and proceed through stepwise removal of halogens from the parent compound. Two different photocatalytic materials have been explored in our laboratories for the reductive dehalogenation of HOCs. For instance, our group has developed a Cu_2O@Pd photocatalyst that demonstrated tandem reductive dehalogenation of both PCBs and PBDEs.[28,43] Based upon the narrow Cu_2O bandgap, visible-light activation of the catalyst was possible, producing H_2 *via* photocatalytic water-splitting. The photo-generated H_2 was subsequently activated on the Pd surface, driving reductive hydrodehalogenation of PBDEs and PCBs.[43] Our results demonstrated that the dehalogenation process exhibited an order of preference for reactivity at the *para* > *meta* ≫ *ortho* positions, where a stepwise dehalogenation process was observed for compounds with multiple halides.[43] More recently, we have developed a multicomponent photocatalyst based on a *m*-$BiVO_4$/BiOBr/Pd nanocomposite that demonstrated substantial photocatalytic activity in the degradation of organic componds.[44] The monoclinic scheelite form of bismuth vanadate (*m*-$BiVO_4$), an n-type semiconductor, has a bandgap energy of 2.4 eV, making it activatable by visible light. Furthermore, BiOBr is a p-type semiconductor with a bandgap of 2.5–2.9 eV. The composite *m*-$BiVO_4$/BiOBr material thus forms a p–n heterojunction favoring increased charge-carrier separation, which is further enhanced by the surface-deposition of Pd nanodomains. This material was shown to be a highly efficient visible-light photocatalyst in the degradation of polychlorinated biphenyls (PCBs).[44]

Herein, we demonstrate a rapid and highly efficient photocatalytic reductive debromination of PBDEs using the *m*-$BiVO_4$/BiOBr/Pd photocatalyst. Our investigation focused on the degradation of BDE-47. BDE-47 is one of the most environmentally significant PBDE congeners, due both to its toxicity and resistance to degradation in the environment.[9,34] Using the *m*-$BiVO_4$/BiOBr/Pd photocatalyst, we achieve rapid and complete degradation of BDE-47 to diphenyl ether, at a rate that is, to the best of our knowledge, significantly higher than in any comparable system thus far reported.

Experimental

Materials

BDE-47 (99.5%) was purchased from Chem Service (West Chester, PA). Bismuth(III) nitrate hydrate (99.999% metals basis), ammonium metavanadate (≥99.995% metals basis), BDE-3 (99%), methanol-[D_4] (99.8% D), 2-propanol (99+%), *t*-butanol (99+%), and ethyl acetate (99%) were obtained from Alfa Aesar (Ward Hill, MA). Reference standard solutions (each 50 μg mL^{-1} in isooctane) of BDE-1, BDE-2, BDE-4, BDE-8, BDE-17, and BDE-28 were purchased from AccuStandard (New Haven, CT). Hexanes (HR-GC grade) were supplied by EMD (Gibbstown, NJ). Palladium acetate (47.5% Pd), cetyltrimethylammonium bromide (≥99%; CTAB), methanol-[D_1] (≥99.0% D), and methanol-[D_3] (99.5% D) were purchased from Acros Organics (Morris Plains, NJ). 1-Propanol (GC, ≥99%) was supplied by Sigma-Aldrich (St. Louis, MO). Absolute ethanol was obtained from Pharmco Aaper (Shelbyville, KY). Acetonitrile (HPLC-LC/MS) was purchased from BDH/VWR International (Radnor, PA).

Ultra-high-purity N_2 and Ar were supplied from Airgas (Miami, FL). Ultra-pure water (18 MΩcm) was produced by a Barnstead E-Pure system (Thermo Fisher Scientific, Waltham, MA). All reagents were used as received without further purification.

Synthesis of *m*-$BiVO_4$/BiOBr and *m*-$BiVO_4$/BiOBr/Pd nanocomposites

The procedure reported by Pálmai *et al.*[44] was used to produce *m*-$BiVO_4$/BiOBr and the Pd-decorated *m*-$BiVO_4$/BiOBr ternary nanocomposite. Briefly, 0.234 g NH_4VO_3 (2 mmol) in 20 mL H_2O was stirred for 10 min at 90 °C, after which the solution was allowed to cool to room temperature. In a separate three-necked flask, 0.730 g (2 mmol) CTAB in 40 mL H_2O was stirred vigorously at 60 °C, as the NH_4VO_3 solution was added dropwise. Next, 1.94 g $Bi(NO_3)_3{\cdot}5H_2O$ (4 mmol) and 20 mL H_2O were placed in a clean flask, and the mixture was agitated in a sonication bath for 2 min, then stirred for a further 10 min. The resulting white suspension was added dropwise to the stirring NH_4VO_3/CTAB mixture, and the temperature was raised to 80 °C. Stirring was continued for 16 h, after which the lemon-yellow *m*-$BiVO_4$/BiOBr product was filtered and washed with water, followed by ethanol, and dried overnight under vacuum at 60 °C.

The palladized composite was prepared by dispersing 0.8 g of the *m*-$BiVO_4$/BiOBr in ~100 mL anhydrous ethanol using an ultrasonic probe for 5 min. After sonication, an additional 300 mL anhydrous ethanol was added to the suspension. The flask was then covered with aluminum foil to exclude light and placed on a magnetic stirrer. In a small test tube, 80 mg $Pd(OAc)_2$ was partially dissolved in ~2 mL ethyl acetate. The $Pd(OAc)_2$ solution was then added to the *m*-$BiVO_4$/BiOBr suspension, and the mixture was stirred overnight in the dark. The dark green product was filtered, washed with anhydrous ethanol, and dried under vacuum at 60 °C.

Characterization of *m*-$BiVO_4$/BiOBr/Pd nanocomposite

The *m*-$BiVO_4$/BiOBr and *m*-$BiVO_4$/BiOBr/Pd materials were characterized by scanning electron microscopy (SEM) using a Philips XL30 field-emission environmental SEM equipped with an Oxford energy-dispersive X-ray detector and by transmission electron microscopy (TEM) using a JEOL JEM-1400 TEM. SEM experiments were conducted at 20 kV, while TEM experiments were run at 80 kV. Complete material characterization, including energy-dispersive spectroscopy (EDS), EDS mapping, EDS line-scanning, high-resolution TEM (HRTEM), powder X-ray diffraction (XRD), X-ray photoelectron spectroscopy (XPS), and UV-visible diffuse reflectance spectroscopy (DRS) was previously published.[44,45]

Photocatalytic debromination of brominated diphenyl ethers

A concentrated stock solution of BDE-47 (in ethanol) was diluted to 25.0 μM using 50 : 50 (v/v) ethanol/water. The solution was then degassed with N_2 for 30 min, from which 50.0 mL of the solution was added to 25 mg of *m*-$BiVO_4$/BiOBr/Pd in a 60 mL borosilicate glass vial with a silicone septum cap and magnetic stir bar. The vial was sealed, sonicated for 30 s, flushed with dry ultra-high purity N_2 for 30 min, and then stirred for 2 h. This was done to ensure that adsorption equilibrium was achieved (see Fig. S2†). The reaction vial was then placed on a stir plate in a photochemical safety cabinet (Ace Glass, Vineland, NJ, model #7836-20) at a distance of 10 cm from a water-cooled 450 W medium-pressure mercury-vapor lamp (Ace Glass #7825-34, light intensity = 60 mW cm^{-2}), based upon manufacturer specification. At selected time points, 500 μL aliquots were taken and combined with equal volumes of high-resolution-GC-grade hexanes in 2 mL vials. The vials were agitated for 1 h on a vortexer to extract the organic products into the hexanes layer. From these extractions, 100 μL samples were spiked with 15 μL of 24 ppm 1,4-dibromo-2,3,5,6-tetrafluorobenzene in hexanes as an internal standard and analyzed using GC/MS (Agilent 5975C GC/MS with HP-5MS column: 30 m length, 0.250 mm ID, 0.25 μm film thickness, Santa Clara, CA).

For the reactions in isotopically labeled solvents, 2.2 μL of 22.8 mM BDE-3 in acetonitrile was deposited in a 1.8 mL GC autosampler vial, and the solvent was evaporated. To this, 2.0 mg *m*-$BiVO_4$/BiOBr/Pd particles was added, along with a flea-size magnetic stir bar and 300 μL of the isotopically labeled methanol. The vial was capped, sealed with parafilm, and flushed with N_2 while stirring vigorously for 5 min. The mixture was exposed to light from the mercury-vapor lamp for 10 min while stirring, after which the solvent was evaporated under N_2 and replaced with 400 μL tetrachloroethylene. The solution was transferred to two 200 μL glass GC vial inserts, each placed in a microcentrifuge tube. These samples were then centrifuged from which an aliquot was extracted and prepared for GC analysis.

Results and discussion

The photocatalytic activities of *m*-$BiVO_4$/BiOBr and *m*-$BiVO_4$/BiOBr/Pd nanocomposites were investigated in the degradation of the polybrominated diphenyl ether, BDE-47. This substrate is frequently the predominant congener detected in human blood and tissue samples, and is specifically implicated in numerous studies of adverse health effects.[9,10,46,47] For example, a significant association was found between prenatal BDE-47 exposure and lower scores on standard developmental indices among children at 12–48 months of age.[48]

The *m*-$BiVO_4$/BiOBr was synthesized using a previously reported facile procedure.[44] Fig. 1a shows an SEM image of the *m*-$BiVO_4$/BiOBr nanocomposite. These materials display clusters of flake-like nanosheets with an average width of 0.70 ± 0.36 μm and average thickness of 33 ± 12 nm (N = 100). Fig. 1b presents a TEM image of the same materials after Pd nanoparticle incorporation to form *m*-$BiVO_4$/BiOBr/Pd. The figure displays Pd particles dispersed on the surface of metal oxide materials. Energy-dispersive X-ray spectroscopy (EDS) (Fig. S1†) confirms separate V-enriched and Br-enriched regions of the composite, corresponding to $BiVO_4$

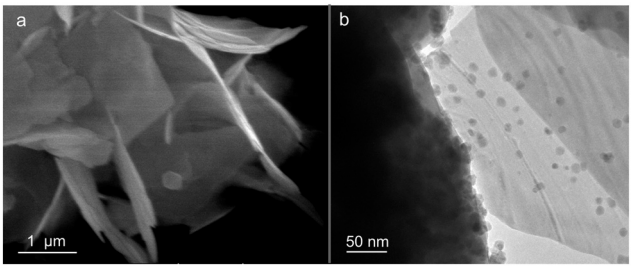

Fig. 1 (a) SEM image of *m*-$BiVO_4$/BiOBr; (b) TEM image of *m*-$BiVO_4$/BiOBr/Pd showing Pd surface decoration.

and BiOBr, respectively. No further characterization of the material was undertaken, as the observed features are consistent with the previously-reported *m*-$BiVO_4$/BiOBr/Pd nanocomposite.[44]

To photocatalytically debrominate the molecule, BDE-47 was commixed with $BiVO_4$/BiOBr/Pd and exposed to light as described in the Experimental section. As shown in Fig. 2a, photocatalytic debromination of BDE-47 using *m*-$BiVO_4$/BiOBr/Pd occurs rapidly. A 25 μM solution of BDE-47 (light blue curve) was completely degraded to diphenyl ether (DPE – red curve) within 40 min of irradiation. The loss of the first Br^- was complete in less than 5 min, where the pseudo-first-order rate constant for this initial step was 1.33 ± 0.11 min^{-1}.

Recent reports of photocatalytic reductive debromination of BDE-47 include using Cu_2O@Pd (debromination rate constant of k_{obs} = 3.5 × 10^{-3} min^{-1}),[43] Cu_2O/TiO_2 (k_{obs} = 0.007 min^{-1}),[49] g-C_3N_4/Pd (0.019 min^{-1}),[50] Ag@Ag_3PO_4/g-C_3N_4/rGO (k_{obs} = 0.11635 min^{-1}),[51] and CuO/TiO_2 (k_{obs} = 0.11–0.41 min^{-1}).[41] In addition, Wang *et al.*[52] studied debromination of BDE-47 on metal-doped TiO_2; while rate constants were not reported, the graphed data for the best system studied implied a k_{obs} of ~0.6 min^{-1} for TiO_2/Pd in pure methanol solvent, with diphenyl ether, dibenzofuran, and assorted mono- and di-bromodiphenyl ethers as the principal products at the conclusion of the experiment. Of these recent examples, the composite Ag@Ag_3PO_4/g-C_3N_4/rGO is the one with the fastest rate of BDE-47 debromination that was also reported to eventually cause complete debromination of BDE-47. The pseudo-first-order rate constant (1.33 ± 0.11 min^{-1}) obtained in the present system demonstrates a significant advancement in reactivity. Such a value is ~380-fold faster than the one observed previously for the Cu_2O@Pd photocatalytic system,[43] an order of magnitude greater than that reported for Ag@Ag_3PO_4/g-C_3N_4/rGO,[51] and more than double the rate reported for TiO_2/Pd in pure methanol.[52]

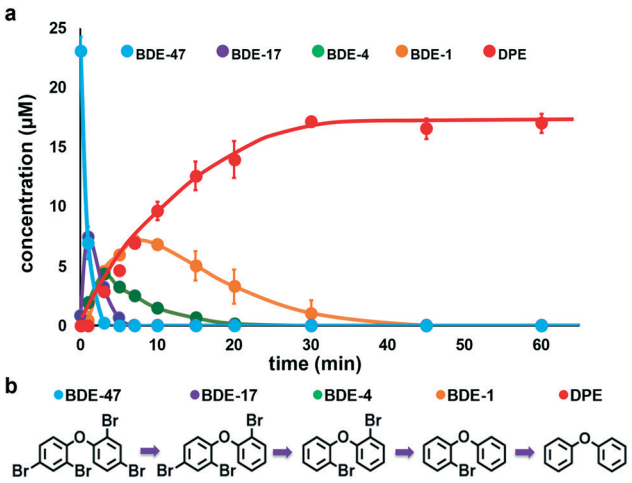

Fig. 2 (a) Photodebromination reaction of BDE-47 under light irradiation with 0.5 mg mL^{-1} *m*-$BiVO_4$/BiOBr/Pd suspension. Error bars represent standard deviation (*n* = 3). (b) Product sequence for dominant pathway.

After 1 min into the reaction, a substantial amount of the tribromo BDE-17 (purple curve) was detected. The concentration of BDE-17 began to decrease from its maximum at this time point, giving rise to the production of the dibromo BDE-4 species (green curve). The concentration of BDE-4 continued to increase until ~5 min, after which the concentration decreased, concomitant with the production of 2-monobromodiphenyl ether, BDE-1 (orange curve). The BDE-1 species reached a maximum concentration at ~9 min of reaction. After this time, it was fully consumed within 40 min to generate the DPE final product.

As indicated by the sequence of products generated in the reactions (Fig. 2b), the reductive degradation of BDE-47 exhibits stepwise debromination, starting with the *para*-bromines on the two benzyl rings. Once these two species are consumed, reactivity at the two *ortho* bromines occurs to generate the bromine-free DPE product. Minor products produced through loss of an *ortho* bromine before a *para* bromine (BDEs 28, 15, 8, and 3) appear briefly, but never exceed a concentration of ~1 μM (less than 4% of the starting material), and they are entirely gone within the first 10 min of the reaction. In addition, a trace of dibenzofuran, too low to be quantified, was detected. These products might be due to a trace level of a concurrent photolysis reaction and are omitted from Fig. 2a for clarity. It is important to note that a stepwise process of removal of a single bromine occurs for all reaction intermediates; the data do not suggest a concerted debromination process that removes two or more bromines simultaneously. This preference for debromination at the *para* position is the reverse of what has been reported for direct photolysis in the absence of catalyst.[53] In the case of direct photolysis, debromination at the *ortho* position is preferred, as is predicted by DFT calculations for the mono-brominated BDEs, showing the *para* bromine to be ~6 kJ mol^{-1} more stable than the *ortho* counterpart.[54] The observed preference for debromination at the *para* position using the *m*-$BiVO_4$/BiOBr/Pd catalyst, however, is consistent with product sequences reported for dehalogenation of PBDEs and PCBs using other Pd-based catalysts.[34,42,43,52,55] This behavior suggests that the debromination mechanism involves direct interaction of the BDE with the Pd surface, where the sterically less-hindered *para* bromine is more accessible, and thus more easily removed than the thermodynamically-favored *ortho* bromine.

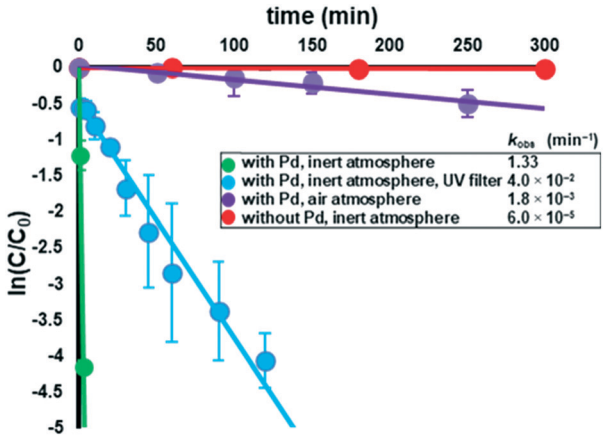

Fig. 3 Degradation of 50 mL 25.0 μM BDE-47 (loss of first Br, $\ln(C/C_0)$ *vs.* *t*) under light irradiation with 0.5 mg mL^{-1} *m*-$BiVO_4$/BiOBr/Pd suspension, and under specified conditions. Error bars represent standard deviation (n = 3). Pseudo-first order rate constants shown.

To confirm the photocatalytic reactivity of the *m*-$BiVO_4$/BiOBr/Pd materials for BDE-47 photodebromination, a variety of control experiments were conducted, as shown in Fig. 3. For these controls, the loss of the first bromine of BDE-47 was monitored over time. Initially, the reactivity of the *m*-$BiVO_4$/BiOBr without surface-deposited Pd was examined. Using these materials in the same reaction set up, negligible photocatalytic debromination was observed; only a trace amount of 2,4,4′-tribromodiphenyl ether (BDE-28) was detected after 300 min (k_{obs} = 6 × 10^{-5} min^{-1}). This level of reactivity, which is 22 000-fold slower than the Pd-decorated materials, can be attributed to direct UV photolysis, consistent with prior results.[43] In addition, when the *m*-$BiVO_4$/BiOBr/Pd materials were used, but in the presence of O_2, greatly diminished reactivity was observed compared to the anaerobic system used for Fig. 2. In this case, minimal BDE-47 degradation was noted, giving rise to a k_{obs} = 1.8 × 10^{-3} min^{-1}. Such effects are likely due to O_2 scavenging electrons and ceasing the catalytic reduction, leaving direct photolysis the dominant path in this case.

Beyond the material composition effects, the contributions of the wavelength of light used to drive the photocatalytic process was explored. To probe this effect, the reaction was irradiated in the light box, but a UV-cutoff filter was used to ensure that only visible light was employed to drive the reaction. As displayed in Fig. 3, under only visible light irradiation (~43% of the mercury lamp's total output is visible light, according to the manufacturer's specification), the ternary composite photocatalyst still exhibited significant catalytic reactivity in the reductive debromination of BDE-47 (k_{obs} = 3.99 × 10^{-2} min^{-1}). Although this rate is slower than when both UV and visible light were used, it is higher than the one previously reported for Cu_2O@Pd using twice the catalyst concentration and no UV filter under otherwise identical conditions.[43] Consequently, both the material structure (*m*-$BiVO_4$/BiOBr/Pd) and the wavelength of light used are critically important in controlling the overall reactivity. It should be noted that significant BDE-47 degradation was observed when using visible light only to drive the reaction. This suggests that solar illumination could be a plausible photoexcitation source, making this ternary composite photocatalyst potentially amenable for environmental remediation under sustainable conditions.

The mechanism of reductive debromination using the *m*-$BiVO_4$/BiOBr/Pd photocatalyst was probed in greater detail using 4-bromodiphenyl ether, BDE-3, as the substrate. This monobrominated congener was chosen to avoid the complication of multistep reactivity evident with polybrominated substrates. In addition, BDE-3 has the bromine substituent at the *para* position on the phenyl ring, which showed the greatest reactivity for photodebromination. Using this substrate, the active species involved in the BDE debromination was identified using selected scavengers in the reaction (Fig. 4). In these experiments, the BDE-3 concentration was 100 μM, whereas the final concentration of added scavenger was 1.0 mM.

For the baseline reaction, BDE-3 was debrominated using *m*-$BiVO_4$/BiOBr/Pd in the absence of added scavengers. For this system, the pseudo-first order rate was 0.22 ± 0.03 min^{-1}, which is more than two orders of magnitude faster than for a previous photocatalytic system for this reaction using the same experimental setup but a different catalyst (Cu_2O/Pd, k_{obs} = 0.0016 min^{-1}).[43] *t*-Butanol,[56–58] EDTA,[58–60] and $(NH_4)_2S_2O_8$ (ref. 61–63) are well-established scavengers for hydroxy radicals, holes, and electrons, respectively. Since the photodebromination reaction was processed under O_2-free conditions, superoxide radicals were highly unlikely to have participated in the reaction. *t*-Butanol was added to the reaction to probe the contribution of hydroxyl radicals in the photocatalytic debromination of BDE-3 by the *m*-$BiVO_4$/BiOBr/Pd ternary photocatalyst. For this reaction, no significant change in reactivity was observed (k_{obs} = 0.28 ± 0.03 min^{-1}) compared to the standard system. This suggests that hydroxyl radicals are not formed in this photocatalytic process. To probe

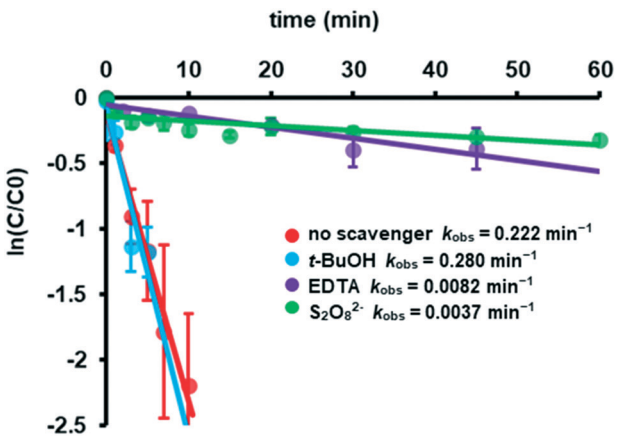

Fig. 4 Effect of scavengers (1.0 mM) on rate of reaction for BDE-3 (100 μM in 1:1 EtOH/H_2O) under light irradiation with 0.5 mg mL^{-1} *m*-$BiVO_4$/BiOBr/Pd suspension. Error bars represent standard deviation (n = 3). Pseudo-first order rate constants shown.

the influence of the charge-carriers in the reaction, two additional scavengers were used: EDTA as a hole scavenger and $(NH_4)_2S_2O_8$ as an electron scavenger. For both cases, the reactivity was substantially inhibited, giving rise to k_{obs} values of 0.0082 ± 0.0028 min^{-1} and 0.0037 ± 0.0007 min^{-1} for the EDTA- and $(NH_4)_2S_2O_8$-scavenged reactions, respectively. This suggests that the electrons and holes generated upon light excitation of the *m*-$BiVO_4$/BiOBr/Pd ternary photocatalyst are directly responsible for the debromination of BDEs.

The pattern of products generated from the photocatalytic debromination of BDE-47 (Fig. 2) indicates that the reaction proceeds *via* a reductive dehalogenation mechanism. In this case, a sacrificial reagent must be present in the reaction system to scavenge the holes generated on the *m*-$BiVO_4$/BiOBr/Pd photocatalyst. In the present system, ethanol serves as the sacrificial reagent and is also used to increase BDE solubility in the reaction medium. The effects of the alcohol identity were thereupon examined (Table S1†) to elucidate two key points: how the position of the alcohol functional group affects reactivity and to resolve which H-atom is transferred from the alcohol molecule to the BDE during debromination. To identify the effect of the alcohol functional group's position, ethanol was substituted in the reaction with either a secondary alcohol (2-propanol) or tertiary alcohol (*t*-butanol). When the photocatalytic debromination of BDE-3 was processed under the standard conditions, no reactivity with *t*-butanol/H_2O was observed, and only trace amounts of DPE were detected after 30 min in 2-propanol/H_2O. Since it was demonstrated in the scavenger study that *t*-butanol added to ethanol/H_2O was not inhibitory, it is concluded that the lack of reactivity here is due to the absence of ethanol. In addition, when acetonitrile/H_2O was used in the reaction, photodebromination was inhibited as well. Interestingly, various primary alcohols, including methanol, ethanol, and 1-propanol, all supported reactivity. Furthermore, when ethanol was added to the CH_3CN/H_2O system that had demonstrated no reactivity, the reactivity was restored, confirming the role of the primary alcohol in the system (solvent ratio after addition = 1 : 1 : 1). GC analysis of the aqueous phase of the 1-propanol and ethanol reaction products prior to hexane extraction indicated the presence of propanal and acetaldehyde, respectively. The low boiling point of acetaldehyde made its quantification under these conditions impractical; however, propanal production in the 1-propanol/H_2O reaction was shown to increase as the photocatalytic reaction proceeded (Fig. S3†). This indicates that the primary alcohols are oxidized to the aldehyde product, likely *via* the holes generated on the *m*-$BiVO_4$/BiOBr/Pd materials during photoexcitation, consistent with the photocatalytic aldehyde formation from alcohols reported for palladized TiO_2.[64–66]

It is important to note that while it is expected that ethanol alone would act as an efficient hole scavenger, it was shown that EDTA, which also scavenges holes had a profound effect that inhibited reactivity. As such, the alcohol does not merely serve to accept holes; when EDTA competes for the holes, it interferes with the reaction. This suggests that the ethanol must participate in the reaction beyond simply scavenging holes. In addition, while *t*-butanol was shown not to inhibit the reaction, it was also observed that when used in place of ethanol, the photodebromination reaction did not proceed. This supports the conclusion that a primary alcohol is required to supply H atoms for the reaction. The formation of acetaldehyde from ethanol, as observed *via* GC-MS in these reactions, requires the loss of both the hydroxyl and α protons. This could be through either sequential reduction and oxidation, or through concerted dehydrogenation.[67] In this case, either of these two H atoms, or both, could be involved in debromination of the BDE. It is thus important to determine the identity of the incorporated H atom, or whether hydroxyl and α protons can participate equally in displacing Br.

To identify which H-atom is transferred from the alcohol molecule to the BDE during the reductive debromination, the reaction was processed using a variety of deuterated methanol compounds as the solvent and sacrificial reagents, including CH_3OD, CD_3OH, and CD_3OD. In these reactions, it is important to note that no H_2O was present, just the neat methanol-based solvent, the DPE substrate, and the photocatalysts. Since the conduction band of $BiVO_4$ at +0.40 V is insufficient for the reduction of H^+ from H_2O, it is assumed that the source of H is the dehydrogenation of the alcohol; however, the deuterated substrates can be used to identify which atom is transferred to better understand the reaction mechanism. For these studies, the endpoint at 10 min light exposure was analyzed for product formation and isotope integration. For each reaction system, the mass spectrum of the resulting DPE product was examined, and the ratio of the abundance A_{171}/A_{170} of the m/z = 171 peak (corresponding primarily to DPE incorporating a D atom) to the m/z = 170 peak (corresponding primarily to DPE without D) was determined (Fig. 5). It should be noted that the magnitudes of these peaks do not exclusively represent the degree of incorporation of deuterium from the isotopically-labeled

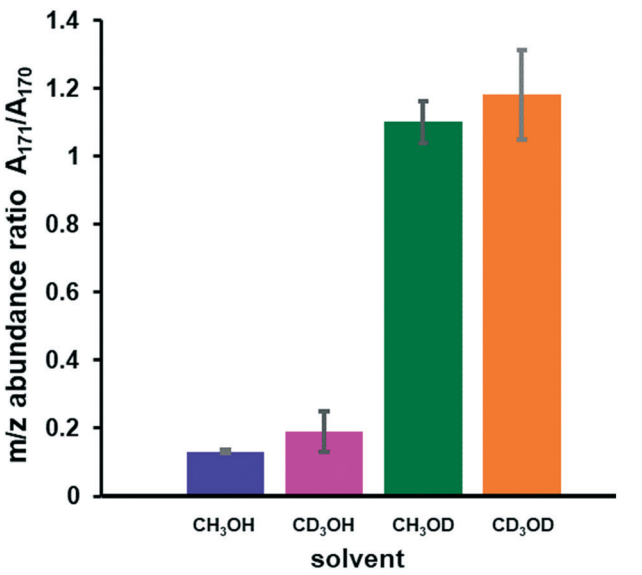

Fig. 5 Mass abundance ratios in product (DPE) of BDE-3 degradation reaction in isotopically-labeled methanol.

solvent, but also reflect the natural abundances of elements including both ^{2}H and ^{13}C. For this reason, only the abundance ratios for the two peaks mentioned above were compared among the DPE products. The ratios were found to be similar when either CH_3OH (A_{171}/A_{170} = 0.13 ± 0.01) or CD_3OH (A_{171}/A_{170} = 0.19 ± 0.06) was the solvent (Fig. 5); however, when the reaction was processed in CH_3OD, a substantially higher degree of deuteration was observed (A_{171}/A_{170} = 1.10 ± 0.06), which was comparable to that obtained with CD_3OD (A_{171}/A_{170} = 1.18 ± 0.13). This suggests that the hydroxyl group H atom is the predominant source of H for bromine substitution in the photodebromination of BDE-3.

Based upon the information obtained from the scavenger, solvent substitution, and deuterium experiments, a possible mechanism can be advanced, as shown in Scheme 1. Upon photoexcitation of the *m*-$BiVO_4$/BiOBr/Pd material, the primary alcohol is oxidized to the corresponding aldehyde. This is achieved by α H atoms of the alcohol being oxidized by photogenerated holes on p-type regions of the catalyst surface (BiOBr), while the more acidic hydroxyl H atoms are reduced by photogenerated electrons accumulated on the Pd domains. This latter step results in H atoms being adsorbed on the Pd, which are then activated to drive BDE debromination, displacing bromine and eventually generating the DPE final product once all the bromine substituents are replaced. In this scheme, only the hydroxyl H atoms would be activated on the Pd metal and incorporated into the DPE product, which is supported by the isotopic labeling experiments. As indicated above, concerted dehydrogenation/hydrodebromination may also possible.

While the mechanism above is driven *via* primary alcohols, the observation that isopropanol offered little or no support for the photocatalytic hydrodebromination of BDE-3 was somewhat surprising, since this alcohol is routinely used as a sacrificial electron donor or hole scavenger in photocatalytic reactions.[68] In search of a possible theoretical explanation for the apparent requirement that the alcohol employed as a sacrificial hole sink be a primary alcohol, a simplified natural bond orbital (NBO)[69] analysis, based on rudimentary DFT calculations,[70] was performed (p. S5†). NBO theory is a powerful tool for deriving insight into chemical bonding and reactivity from electronic structure calculations.[71,72] Selected results are listed in Table S2,† along with the alcohols' pK_a values,[73] for reference.

Comparing the minimum natural charge on an α H for each of the alcohols (Table S2,† shaded column) reveals that 2-propanol, the only alcohol among the group that does not readily support the catalytic reaction, has a noticeably higher charge. The more positively charged α-H of the secondary alcohol is thus repelled more strongly by the photogenerated holes on the catalyst surface, reducing the opportunity for C–H_α bond – h^+ interaction. Furthermore, the calculated

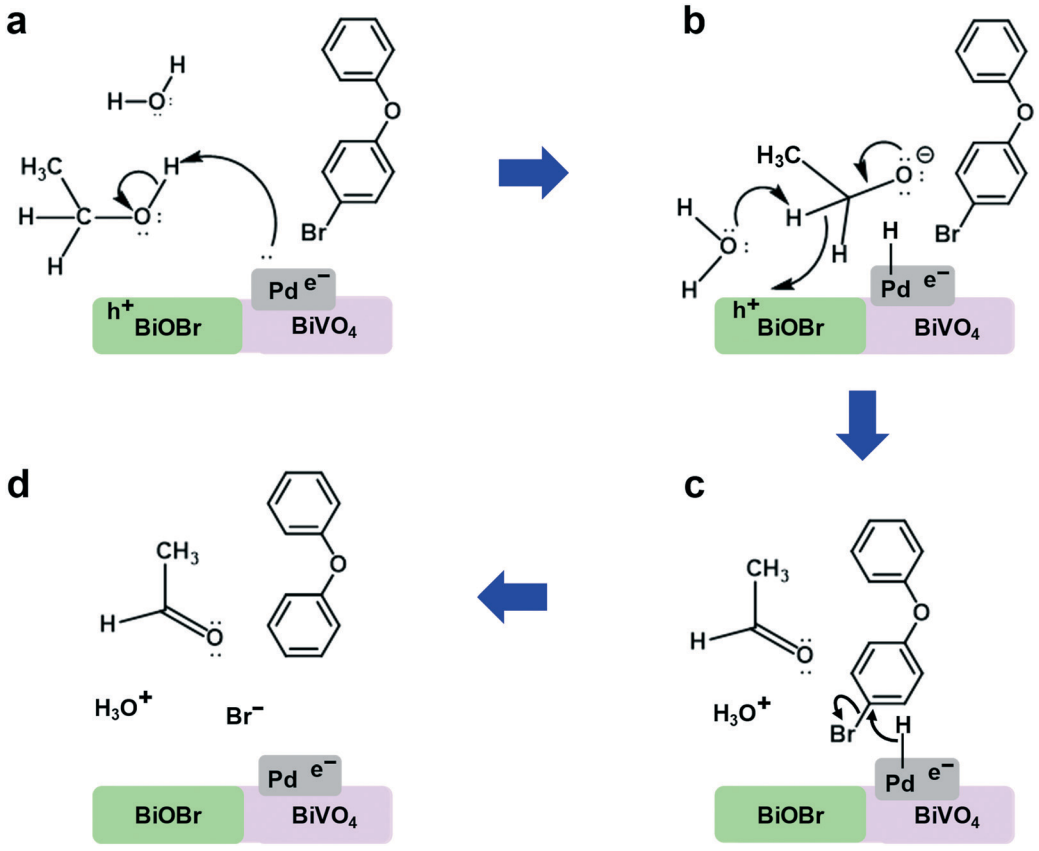

Scheme 1 Possible mechanism for (a and b) oxidative dehydrogenation of ethanol; (c and d) hydro-debromination of BDE-3.

interactions between oxygen lone pairs and C–H_α antibonding orbitals would serve to weaken those C–H_α bonds in the primary alcohols. In the lowest-energy conformation of the secondary alcohol, however, the only significant donor–acceptor interactions involve C–C antibonding orbitals. Moreover, from the pK_a values, it can be seen that the hydroxyl hydrogens of the primary alcohols are more labile than that of the secondary alcohol.

For the second part of the mechanism, hydrodebromination by Pd-adsorbed H atoms, this is consistent with the observed preference for debromination of BDE-47 at the *para* position. Whereas the thermodynamically-favored removal of an *ortho* Br is preferred in direct photolysis by UV light in the absence of catalyst, steric considerations in the interaction of BDE-47 with the active surface favor Br loss at the *para* position in the catalyzed reaction. For a pathway in which an intermediate reactive species (*e.g.*, a radical) were responsible for debromination, *ortho* preferred reactivity would be expected. Since both the first and second Br lost from BDE-47 are almost exclusively at the *para* positions, the reaction catalyzed by the *m*-$BiVO_4$/BiOBr/Pd composite may suggest a surface-based mechanism, wherein reaction at the least sterically-hindered position dominates.

This surface-dependency of the mechanism is integral to one of the key advantages of *m*-$BiVO_4$/BiOBr/Pd as a photocatalyst for the debromination of PBDEs: it avoids producing the dangerous by-products that can be generated through radical-based mechanisms.[35–37] Furthermore, this work has shown that *m*-$BiVO_4$/BiOBr/Pd completely debrominates BDE-47, one of the BDEs most recalcitrant to degradation, to the relatively benign diphenyl ether, leaving no brominated organic products. Moreover, this was achieved at a rate significantly faster than has been reported for other photocatalysts;[41,51,52] as such, we believe *m*-$BiVO_4$/BiOBr/Pd provides a significant advancement in photocatalytic degradation of PBDEs.

Conclusions

A ternary composite nanomaterial photocatalyst, *m*-$BiVO_4$/BiOBr/Pd, was successfully used to drive photocatalytic debromination of 2,2′,4,4′-tetrabromodiphenyl ether (BDE-47) to the final DPE product. The reaction was conducted under highly sustainable conditions using light as the energy source for the reaction. In addition, the nanocomposite catalyst was produced by a simple, surfactant-assisted synthesis without the need for high-temperature processing such as calcination, further enhancing the overall synthesis and use of the materials. The mechanism of the photocatalytic hydrodebromination was investigated in detail. For this, oxidation of a primary alcohol occurs first, positioning the H-atom of the alcohol functional group onto the Pd nanodomain. This newly activated H-atom subsequently reacts with the BDE, leading to debromination. Such atomic level mechanistic detail provides greater understanding of how the material structure affects the reactivity, allowing for enhanced material design. Such capabilities provide intriguing opportunities for the design, development, and eventual deployment of novel catalytic systems for solar-based degradation of environmental pollutants, which is a pressing goal in light of the current global persistence of PBDEs in the environment.

Author contributions

Conceptualization, methodology, writing – review & editing: EM, EZ, MK, LB. Investigation, formal analysis, software, visualization, writing – original draft: EM. TEM characterization: EZ.

Conflicts of interest

There are no conflicts to declare.

Acknowledgements

The authors are grateful to Dr. Patricia Blackwelder, University of Miami Center for Advanced Microscopy, for SEM and TEM analyses, and to Dr. Orlando Acevedo, University of Miami, for guidance with theoretical calculations. This material is based upon work partially supported by the National Science Foundation under Grant No. (CHE-1903649 – MRK).

Notes and references

1 M. A. Ashraf, *Environ. Sci. Pollut. Res.*, 2017, **24**, 4223–4227.
2 M. A. Han, J. H. Kim and H. S. Song, *Eur. J. Cancer Prev.*, 2019, **28**, 344–349.
3 P. D. Jepson and R. J. Law, *Science*, 2016, **352**, 1388–1389.
4 *Stockholm Convention on Persistent Organic Pollutants (POPS)*, Secretariat of the Stockholm Convention (SSC), United Nations Environment Programme (UNEP), Châtelaine GE – Switzerland, 2018.
5 V. Zitko, in *Persistent Organic Pollutants*, 2003, ch. 4, pp. 47–90, DOI: 10.1007/10751132_4.
6 L. W. Robertson and G. Ludewig, *Gefahrstoffe - Reinhalt. Luft*, 2011, **71**, 25–32.
7 C. A. de Wit, *Chemosphere*, 2002, **46**, 583–624.
8 EPA, *An Exposure Assessment of Polybrominated Diphenyl Ethers (PBDE) (Final Report) U.S. Environmental Protection Agency*, Washington, DC, EPA/600/R-08/086F, 2010, URL: http://cfpub.epa.gov/ncea/risk/recordisplay.cfm?deid=210404, (accessed 12/07/2020).
9 Z. Wu, C. He, W. Han, J. Song, H. Li, Y. Zhang, X. Jing and W. Wu, *Environ. Res.*, 2020, **187**, 109531.
10 V. Linares, M. Belles and J. L. Domingo, *Arch. Toxicol.*, 2015, **89**, 335–356.
11 A. Q. Shan, M. X. Li, X. J. Li, Y. Y. Li, M. F. Yan, P. Xian, Y. Chang, X. Chen and N. J. Tang, *Chem. Res. Toxicol.*, 2019, **32**, 621–628.
12 V. M. Richardson, D. F. Staskal, D. G. Ross, J. J. Diliberto, M. J. DeVito and L. S. Birnbaum, *Toxicol. Appl. Pharmacol.*, 2008, **226**, 244–250.

13 L. G. Costa and G. Giordano, *Neurotoxicology*, 2007, **28**, 1047–1067.
14 G. Y. Xu and J. B. Wang, *Chemosphere*, 2014, **110**, 70–77.
15 H. Stiborova, J. Vrkoslavova, P. Lovecka, J. Pulkrabova, P. Hradkova, J. Hajslova and K. Demnerova, *Chemosphere*, 2015, **118**, 315–321.
16 A. Rein, M. M. Fernqvist, P. Mayer, S. Trapp, M. Bittens and U. G. Karlson, *Appl. Microbiol. Biotechnol.*, 2007, **77**, 469–481.
17 X. Tang, M. Z. Hashmi, B. Zeng, J. Yang and C. Shen, *Chem. Eng. J.*, 2015, **279**, 673–680.
18 G. Fang, J. Gao, D. D. Dionysiou, C. Liu and D. Zhou, *Environ. Sci. Technol.*, 2013, **47**, 4605–4611.
19 Y. Zhuang, S. Ahn and R. G. Luthy, *Environ. Sci. Technol.*, 2010, **44**, 8236–8242.
20 Z. Liu, F. Zhang, S. K. Hoekman, T. Liu, C. Gai and N. Peng, *ACS Sustainable Chem. Eng.*, 2016, **4**, 3261–3267.
21 V. Rybnikova, M. Usman and K. Hanna, *Environ. Sci. Pollut. Res.*, 2016, **23**, 17035–17048.
22 A. Christiansson, J. Eriksson, D. Teclechiel and A. Bergman, *Environ. Sci. Pollut. Res.*, 2009, **16**, 312–321.
23 N. Matykiewiczova, J. Klanova and P. Klan, *Environ. Sci. Technol.*, 2007, **41**, 8308–8314.
24 G. Söderström, U. Sellström, C. A. de Wit and M. Tysklind, *Environ. Sci. Technol.*, 2004, **38**, 127–132.
25 J. Eriksson, N. Green, G. Marsh and Å. Bergman, *Environ. Sci. Technol.*, 2004, **38**, 3119–3125.
26 C. G. Jones, J. Silverman, M. Al-Sheikhly, P. Neta and D. L. Poster, *Environ. Sci. Technol.*, 2003, **37**, 5773–5777.
27 M. Altarawneh, A. Saeed, M. Al-Harahsheh and B. Z. Dlugogorski, *Prog. Energy Combust. Sci.*, 2019, **70**, 212–259.
28 E. M. Zahran, N. M. Bedford, M. A. Nguyen, Y. J. Chang, B. S. Guiton, R. R. Naik, L. G. Bachas and M. R. Knecht, *J. Am. Chem. Soc.*, 2014, **136**, 32–35.
29 R. K. Wang, X. Q. Ma, T. Liu, Y. C. Li, L. Song, S. C. Tjong, L. X. Cao, W. Wang, Q. Yu and Z. W. Wang, *Appl. Catal., A*, 2020, **597**, 117547.
30 R. Ahmad, Z. Ahmad, A. U. Khan, N. R. Mastoi, M. Aslam and J. Kim, *J. Environ. Chem. Eng.*, 2016, **4**, 4143–4164.
31 J. Wen, X. Li, W. Liu, Y. Fang, J. Xie and Y. Xu, *Chin. J. Catal.*, 2015, **36**, 2049–2070.
32 X. Yang and D. Wang, *ACS Appl. Energy Mater.*, 2018, **1**, 6657–6693.
33 S. G. Kumar and K. S. R. K. Rao, *Appl. Surf. Sci.*, 2017, **391**, 124–148.
34 M. S. Santos, A. Alves and L. M. Madeira, *Water Res.*, 2016, **88**, 39–59.
35 T. An, J. Chen, G. Li, X. Ding, G. Sheng, J. Fu, B. Mai and K. E. O'Shea, *Catal. Today*, 2008, **139**, 69–76.
36 L. Birnbaum, *Environ. Int.*, 2003, **29**, 855–860.
37 P. R. Erickson, M. Grandbois, W. A. Arnold and K. McNeill, *Environ. Sci. Technol.*, 2012, **46**, 8174–8180.
38 F. Alonso, I. P. Beletskaya and M. Yus, *Chem. Rev.*, 2002, **102**, 4009–4092.
39 J. He, K. R. Robrock and L. Alvarez-Cohen, *Environ. Sci. Technol.*, 2006, **40**, 4429–4434.
40 Y.-S. Keum and Q. X. Li, *Environ. Sci. Technol.*, 2005, **39**, 2280–2286.
41 M. Lei, N. Wang, L. Zhu, Q. Zhou, G. Nie and H. Tang, *Appl. Catal., B*, 2016, **182**, 414–423.
42 B. Z. Wu, H. Y. Chen, S. J. Wang, C. M. Wai, W. Liao and K. Chiu, *Chemosphere*, 2012, **88**, 757–768.
43 E. B. Miller, E. M. Zahran, M. R. Knecht and L. G. Bachas, *Appl. Catal., B*, 2017, **213**, 147–154.
44 M. Pálmai, E. M. Zahran, S. Angaramo, S. Balint, Z. Paszti, M. R. Knecht and L. G. Bachas, *J. Mater. Chem. A*, 2017, **5**, 529–534.
45 M. O. Olagunju, E. M. Zahran, J. M. Reed, E. Zeynaloo, D. Shukla, J. L. Cohn, B. Surnar, S. Dhar, L. G. Bachas and M. R. Knecht, *ACS Appl. Nano Mater.*, 2021, **4**, 3262–3272.
46 L. S. Birnbaum and D. F. Staskal, *Environ. Health Perspect.*, 2004, **112**, 9–17.
47 M. Petreas, J. She, F. R. Brown, J. Winkler, G. Windham, E. Rogers, G. Zhao, R. Bhatia and M. J. Charles, *Environ. Health Perspect.*, 2003, **111**, 1175–1179.
48 J. B. Herbstman, A. Sjodin, M. Kurzon, S. A. Lederman, R. S. Jones, V. Rauh, L. L. Needham, D. Tang, M. Niedzwiecki, R. Y. Wang and F. Perera, *Environ. Health Perspect.*, 2010, **118**, 712–719.
49 Z. Hu, X. Wang, H. T. Dong, S. Y. Li, X. K. Li and L. S. Li, *J. Hazard. Mater.*, 2017, **340**, 1–15.
50 M. Lei, Z. Wang, L. Zhu, W. Nie and H. Tang, *Appl. Catal., B*, 2020, **261**, 118236.
51 C. Liang, L. Zhang, H. Guo, C. G. Niu, X. J. Wen, N. Tang, H. Y. Liu, Y. Y. Yang, B. B. Shao and G. M. Zeng, *Chem. Eng. J.*, 2019, **361**, 373–386.
52 R. Wang, T. Tang, Y. C. Wei, D. Dang, K. B. Huang, X. W. Chen, H. Yin, X. Q. Tao, Z. Lin, Z. Dang and G. N. Lu, *Environ. Int.*, 2019, **127**, 5–12.
53 Y. Pan, D. C. W. Tsang, Y. Wang, Y. Li and X. Yang, *Chem. Eng. J.*, 2016, **297**, 74–96.
54 X. Zeng, P. K. Freeman, Y. V. Vasil'ev, V. G. Voinov, S. L. Simonich and D. F. Barofsky, *J. Chem. Eng. Data*, 2005, **50**, 1548–1556.
55 E. M. Zahran, D. Bhattacharyya and L. G. Bachas, *Chemosphere*, 2013, **91**, 165–171.
56 Z. Kozmér, E. Takács, L. Wojnárovits, T. Alapi, K. Hernádi and A. Dombi, *Radiat. Phys. Chem.*, 2016, **124**, 52–57.
57 S. Kim, H. Park and W. Choi, *J. Phys. Chem. B*, 2004, **108**, 6402–6411.
58 T. Li, X. Hu, C. Liu, C. Tang, X. Wang and S. Luo, *J. Mol. Catal. A: Chem.*, 2016, **425**, 124–135.
59 T. Liu, L. Wang, X. Lu, J. Fan, X. Cai, B. Gao, R. Miao, J. Wang and Y. Lv, *RSC Adv.*, 2017, **7**, 12292–12300.
60 Q. Zhang, L. Jiang, J. Wang, Y. Zhu, Y. Pu and W. Dai, *Appl. Catal., B*, 2020, **277**, 119122.
61 Y. Wang and P. Zhang, *J. Hazard. Mater.*, 2011, **192**, 1869–1875.
62 K. Govindan, H. T. Chandran, M. Raja, S. U. Maheswari and M. Rangarajan, *J. Photochem. Photobiol., A*, 2017, **341**, 146–156.
63 M. N. Chong, B. Jin, C. W. Chow and C. Saint, *Water Res.*, 2010, **44**, 2997–3027.
64 Y. Chen, Y. Wang, W. Li, Q. Yang, Q. Hou, L. Wei, L. Liu, F. Huang and M. Ju, *Appl. Catal., B*, 2017, **210**, 352–367.

65 P. A. Kolinko, D. S. Selishchev and D. V. Kozlov, *Theor. Exp. Chem.*, 2015, **51**, 96–103.
66 J. Chen, D. F. Ollis, W. H. Rulkens and H. Bruning, *Water Res.*, 1999, **33**, 669–676.
67 H. F. Wang and Z. P. Liu, *J. Am. Chem. Soc.*, 2008, **130**, 10996–11004.
68 P. V. Kamat and S. Jin, *ACS Energy Lett.*, 2018, **3**, 622–623.
69 F. Weinhold, *J. Comput. Chem.*, 2012, **33**, 2363–2379.
70 A rigorous DFT analysis of the system similar to that done by Wang *et al.* would be of much interest, but is far beyond the scope of the present work.
71 A. E. Reed, R. B. Weinstock and F. Weinhold, *J. Chem. Phys.*, 1985, **83**, 735–746.
72 F. Weinhold, *Discovering chemistry with natural bond orbitals*, Wiley, Hoboken, NJ, 2012.
73 J. F. Stoddart, D. H. Barton, W. D. Ollis, P. G. Sammes, I. Sutherland, D. N. Jones, E. Haslam and C. Drayton, *Comprehensive Organic Chemistry, the Synthesis and Reactions of Organic Compounds*, Chairman and Deputy Chairman of the Ed. Board: Derek Barton and W. David Ollis, Pergamon Press, 1979.